Asymmetric Membrane Capacitive Deionization using Anion-Exchange Membranes based on Quaternized Polymer Blends

Asymmetric Membrane Capacitive Deionization using Anion-Exchange Membranes based on Quaternized Polymer Blends

Robert McNair,[a,b] Levente Cseri,[a] Gyorgy Szekely,[,a,c] & Robert Dryfe[*,b,d,e]*

[a] Department of Chemical Engineering & Analytical Science, University of Manchester, The Mill, Sackville Street, Manchester, M1 3BB, UK
[b] Department of Chemistry, University of Manchester, Oxford Road, Manchester, M13 9PL, UK
[c] King Abdullah University of Science and Technology (KAUST), Advanced Membranes and Porous Materials Center (AMPMC), Thuwal, 23955-6900, Saudi Arabia
[d] National Graphene Institute, University of Manchester, Booth Street East, Manchester, M13 9PL, UK
[e] Henry Royce Institute for Advanced Materials, University of Manchester, Oxford Road, Manchester, M13 9PL, UK

ACS Applied Polymer Materials, https://doi.org/10.1021/acsapm.0c00432

[*]**Corresponding Authors**
Gyorgy Szekely: gyorgy.szekely@kaust.edu.sa, Tel: + 966 128082769
Robert Dryfe: robert.dryfe@manchester.ac.uk, Tel: + 44 (0) 161-306-4522

Graphical Abstract

Anion-exchange membranes fabricated from quaternized polymer blends of polybenzimidazole (PBI) and polyethylenimine (PEI) exhibited a high ion-exchange capacity (IEC) of up to 2.6 mmol g^{-1}, combined with good permselectivity (0.86) and low area resistance (1.5 Ω cm^2) for water desalination through membrane capacitive deionization (MCDI).

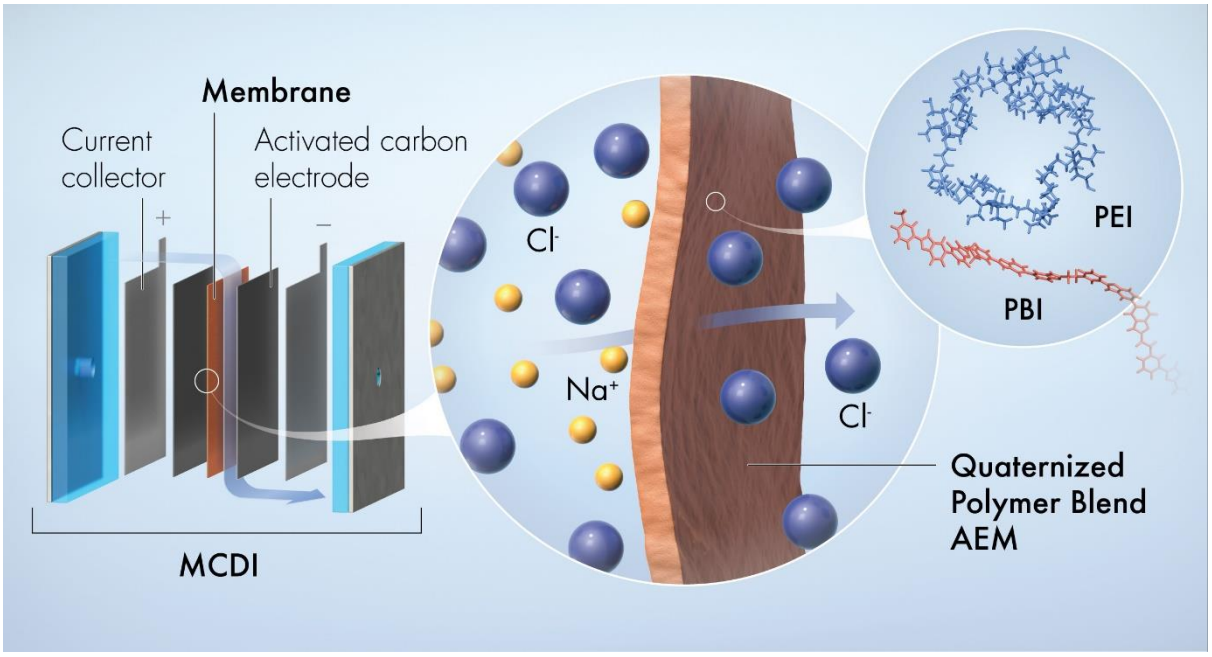

Abstract

Membrane capacitive deionization (MCDI) for water desalination is an innovative technique that could help to solve the global water scarcity problem. However, the development of the MCDI field is hindered by the limited choice of ion-exchange membranes. Desalination by MCDI removes the salt (solute) from the water (solvent); which can drastically reduce energy consumption compared to traditional desalination practices such as distillation. Herein, we outline the fabrication and characterization of quaternized anion-exchange membranes (AEMs) based on polymer blends of polyethylenimine (PEI) and polybenzimidazole (PBI) that provides an efficient membrane for MCDI. Flat sheet polymer membranes were prepared by solution casting, heat treatment and phase inversion, followed by modification to impart anion-exchange character. Scanning electron microscopy (SEM), atomic force microscopy (AFM), nuclear magnetic resonance (NMR) and Fourier-Transform infrared (FTIR) spectroscopy were used to characterize the morphology and chemical composition of the membranes. The as-prepared membranes displayed high ion-exchange capacity (IEC), hydrophilicity, permselectivity and low area resistance. Due to the addition of PEI, the high density of quaternary ammonium groups increased the IEC and permselectivity of the membranes, while reducing the area resistance relative to pristine PBI AEMs. Our PEI/PBI membranes were successfully employed in asymmetric MCDI for brackish water desalination and exhibited an increase in both salt adsorption capacity (>3x) and charge efficiency (>2x) relative to membrane-free CDI. The use of quaternized polymer blend membranes could help to achieve the greater realization of industrial scale MCDI.

Keywords

Anion-exchange membrane, quaternization, polymer blend, water desalination, membrane capacitive deionization, water purification

1. Introduction

The availability of potable water is one of the world's most pressing global challenges. Currently, more than 2 billion people live in countries experiencing high water stress and up to 4 billion people experience severe water scarcity for at least one month each year.[1] Desalination – the removal of salt from saline water – can help to relieve water stress in some areas of the world. Indeed, various countries have installed industrial-scale desalination plants to augment existing water resources.[2] However, existing desalination processes such as multi-stage flash distillation, multi-effect distillation, and mechanical vapor compression all suffer from the need for high electrical, mechanical or thermal energy input leading to high energy consumption and capital cost. Reverse osmosis (RO) is generally considered the benchmark desalination technology in terms of salt removal and energy efficiency, however it also relies on the use of high pressures to generate pure water.[3] Reducing the energy input and capital costs of desalination has therefore attracted huge research interest in recent years.

Capacitive deionization (CDI) has recently emerged as an environmentally friendly and energy efficient route to desalination of brackish water supplies.[4] Although at present CDI is not competitive with RO as a stand-alone technology, it has shown promising results to improve the efficiency of hybrid desalination processes.[5] Conventional CDI operation passes a feed salt solution between two porous electrodes. The exploitation of the ionic charge of the solute allows the ions to be electrosorbed in electric double layers (EDLs) in the electrode pores, by application of a voltage between the two electrodes with opposite polarity.[6] The electrodes are then regenerated by reversing or zeroing the voltage. Electrode architectures based on activated carbon,[7] carbon aerogels,[8] carbon nanotubes (CNTs)[9] and graphene[10] have been extensively studied for electrosorptive ion removal in CDI, owing to their high specific surface areas for ion adsorption. Electrode materials can also be 'faradaic' in nature; such electrodes have the potential to enhance ion removal due to rapid charge-transfer (redox processes) at the electrode's surface. Transition metal dichalcogenides (TMDs)[11] and MXenes[12] have both been employed as CDI electrodes for desalination purposes, while redox-polymer electrodes such as poly(vinyl)ferrocene/carbon nanotubes (PVF-CNT) have shown great success in electrochemically-driven separations of arsenic[13] and organic pollutants[14] from aqueous solutions.

Alternatively, enhanced CDI performance can be achieved through the use of ion-exchange membranes over the electrodes. Typical membrane capacitive deionization (MCDI) utilizes anion- and cation-exchange membranes over the anode and cathode, respectively. Such membranes allow counter-ions to pass

through the electrode/membrane without obstruction, whereas co-ions (ions of the same polarity as the electrode) are blocked. Co-ion expulsion from electrodes can deplete the salt removal and energy efficiency of an (M)CDI system.[15] Ion- selective membranes can reduce co-ion effects, while simultaneously protecting electrodes from potentially damaging parasitic reactions.[16] A study found that MCDI has the potential to be more energy efficient than RO for water salinities of less than 2 g L^{-1}.[17] However, the lack of suitable and inexpensive commercial membrane materials means that practical use of MCDI is seldom realized.

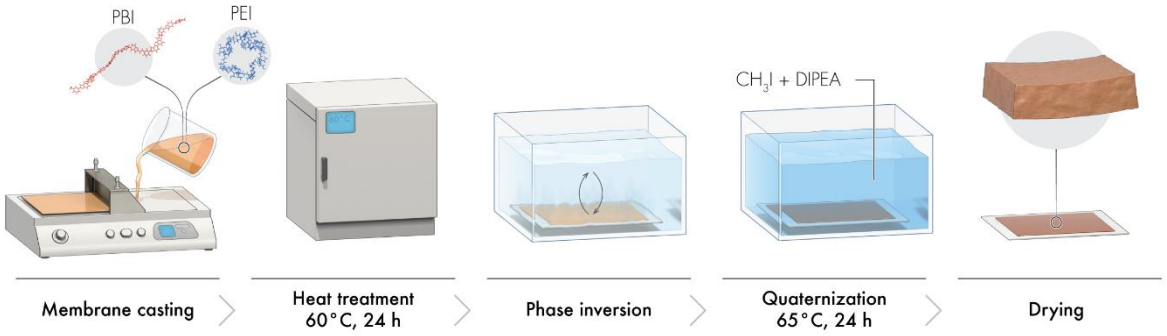

Figure 1. Complete fabrication procedure of quaternized PBI/PEI polymer blend anion-exchange membranes (AEMs) used in this study.

Ideal ion-exchange membranes for MCDI should possess high ion-exchange capacity (IEC) and high permselectivity, combined with a low area resistance and material cost. The reduction of material and operational costs has prompted the use of asymmetric MCDI, which employs anion-exchange membranes (AEMs) over the anode only. Indeed, protection of the anode has been shown to be pertinent to long-term MCDI operation due to oxidation reactions degrading the anode.[18] Successful brominated poly-phenylene oxide (b-PPO) AEMs have been fabricated for MCDI, with reported high desalination performance and high cycling stability.[19] Similarly, AEMs for MCDI were fabricated by polymerization of 4-(chloromethyl) styrene (CMS) monomer in a porous polyethylene substrate. These AEMs achieved a high salt adsorption capacity (16.1 mg g^{-1}) when utilized in MCDI combined with a commercial (CMX) cation-exchange membrane.[20] Cross-linked quaternized polyvinyl alcohol (q-PVA) AEMs with high IEC have been prepared for MCDI, yielding a salt adsorption capacity of 15.6 mg g^{-1} with a NaCl concentration of 800 mg L^{-1}.[21] Nanocomposite AEMs for MCDI based on reduced graphene oxide/polyaniline have also been fabricated, displaying maximum sorption capacity of 1.56 mg g^{-1}. However, these nanocomposite membranes relied on the use of expensive reduced graphene oxide nanofiller material.[22] In this study,

asymmetric MCDI with an AEM over the anode was studied. This allowed us to quantify the degree of improvement, due to the AEMs, on the performance relative to CDI, without the contribution of a CEM.

Here, we describe a simple fabrication procedure (Figure 1) for polymer blend membranes based on polybenzimidazole (PBI) and branched polyethylenimine (PEI). In this procedure, these polymers are quaternized post-casting to impart anion-exchange characteristics. Both of these polymers possess an abundance of aliphatic and aromatic amine groups that are amenable to quaternization to produce quaternary ammonium cations within the membranes, resulting in high IEC.[23] PEI has been employed as a membrane filler in polyethersulfone (PES) for the removal of organic dyes in water treatment by nanofiltration,[24] as well as being used as an additive to carbon nanotube (CNT) electrodes in CDI; resulting in improved performance over conventional CDI and that of commercial anion- and cation-exchange membranes.[25] We hypothesized that the introduction of quaternized PEI embedded in a quaternized PBI matrix would increase IEC, reduce ionic resistance and produce AEMs with a high permselectivity to transport chloride (Cl^-) ions. Increased IEC is usually accompanied by an increase in swelling which reduces resistance, but simultaneously reduces permselectivity as more solution is absorbed by the membrane. This effect can be limited by reducing the film thickness; the ionic resistance is reduced due to the shorter distance across which ions must diffuse, while permselectivity is not sacrificed due to the smaller volume of membrane which undergoes swelling.[26] As a result, the thickness of our membranes (30–40 μm) was reduced by up to 70% compared to commercially available Neosepta AEMs (100–150 μm).[27] We proposed that these factors would help to maintain high ion-exchange and permselective properties of the membranes; facilitating (Cl^-) transport across the membranes into the electrode pores, and increasing the salt removal and energy efficiency of the MCDI systems.

Recently, thin-film composite membranes for organic solvent nanofiltration were synthesized by cross-linking PEI onto PBI substrates.[28] In another study, a nanophase separation structure was created in membranes for vanadium flow batteries by grafting PEI onto a PBI backbone.[29] However, to our knowledge, no results have been reported for the use of PBI/PEI composite polymer blend AEMs for desalination applications. Here, we report on the fabrication of a highly quaternized polymer blend based on PBI/PEI and its application as an AEM in MCDI for water desalination. We describe the full characterization of membrane structure and the determination of their electrochemical properties. We quantified the MCDI performance in terms of salt adsorption capacity and charge efficiency; and compared our results with conventional CDI (without membranes) and relevant MCDI studies.

2. Experimental Section

2.1. Materials

Branched polyethylenimine (PEI, M_W = 25,000 Da), iodomethane (MeI, >99%), *N*-ethyldiisopropylamine (DIPEA, >98%) and dimethyl sulfoxide-d_6 (DMSO-d_6, 99.9%) were all purchased from Sigma-Aldrich. *N,N*-dimethylacetamide (DMAc, > 99.5%) and potassium nitrate (KNO_3, 99+%) were purchased from Acros. Silver nitrate ($AgNO_3$, 99.7%) and acetonitrile (CH_3CN, >99.5%) was purchased from Fisher Scientific. Poly[2,2'-(*m*-phenylene)-5,5'-bisbenzimidazole] (PBI) S26 solution (26 wt% in DMAc solvent) was purchased from PBI Performance Products. YEC-8A activated carbon powder (surface area >2000 $m^2\ g^{-1}$, average particle size = 10 µm) was purchased from Fuzhou Yihuan Carbon Company,[30] carbon black (Super P Conductive Additive) was purchased from Alfa Aesar and polyvinylidine fluoride (PVDF, Kynar 761) binder was purchased from Arkema. Graphite foil current collector (99%) was purchased from Gee Graphite Ltd.

2.2. Membrane Preparation

Table 1 provides the compositions of casting solutions used to prepare membranes. Membranes of PEI content up to a maximum of 20 wt% were fabricated, ensuring nitrogen content (PEI amine groups) could be varied while maintaining the same material processing steps. Firstly, a given amount of PEI and PBI dope solution (26 wt% in DMAc) were separately added to a vessel. A total of 3 g of polymer was used to prepare all membranes. The dope solution was further diluted to the required polymer wt% with DMAc solvent. The mixture was sonicated for 30 minutes to dissolve PEI into the solvent, followed by mixing with an overhead stirrer (6 h, 60 rpm) to homogenize the mixture. The dope solution was then rolled (1 h, 60 rpm) and degassed for 12 hours using an incubator/shaker (40 ℃, 300 rpm). The dope solution was cast at 40℃ on a glass plate to a thickness of 200 µm using an Elcometer 4340 Film Applicator. The membrane was placed in an oven (60 ℃, 24 h) to evaporate solvent and promote the formation of a dense film layer. The membranes were precipitated by immersion in DI water (0.008 L cm^{-2}) resulting in the membrane detaching from the glass plate.

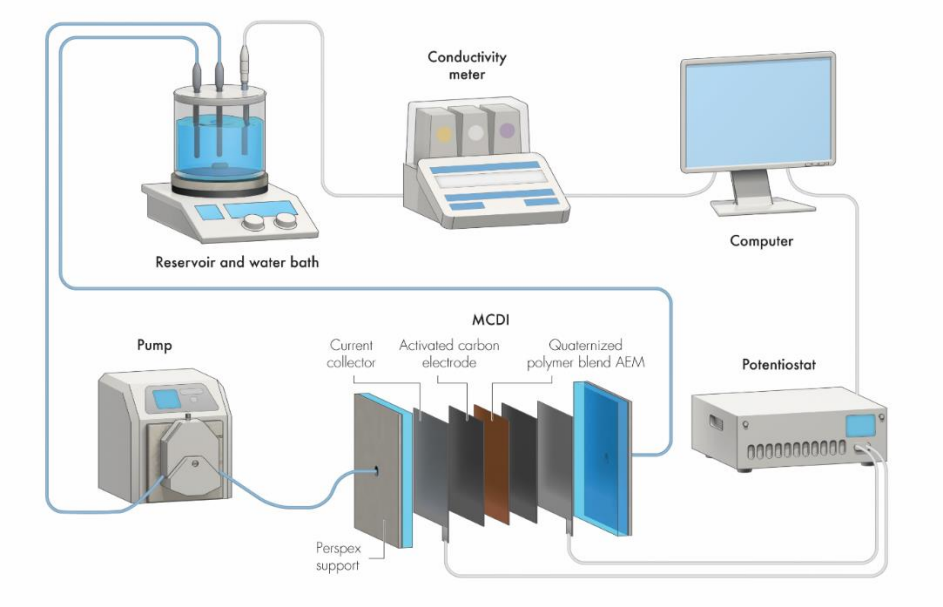

Figure 2. Experimental setup used in this study to conduct batch-mode MCDI.

2.3. Quaternization of Membranes

Quaternization of the prepared membranes was carried out via methylation after membrane casting, as adopted in our previous work.[31] Membrane samples (area 625 cm^2) were rinsed with acetonitrile and placed into a glass pressure tube that had been filled by Ar. The membrane was submerged in acetonitrile (60 mL) and DIPEA (1.4 mL, 8 mM) was added to the solvent, followed by purging with Ar for 5 minutes. Iodomethane (MeI, 2 mL, 32.1 mM) was added and the pressure tube was sealed with an O-ring. The solution was heated at 65 °C under constant stirring for 24 h. The membranes were rinsed sequentially with water and acetonitrile and stored in water/acetonitrile mixture to avoid bacterial growth. Anion substitution (iodide to chloride) was carried out by immersing the membranes into a brine solution for 24 h (40 g L^{-1}) to condition the membrane for desalination applications.

Table 1. Composition of dope solutions and membrane designations used in this study. The quaternization was performed over 24 h using MeI (2 mL, 32 mM) solution.

Membrane	PBI (wt%)	PEI (wt%)	DMAc (wt%)	Total Polymer (wt%)	Mass Ratio (PBI:PEI)
Q0	20.0	0.0	80.0	20.0	100:0
Q5	19.0	1.0	80.0	20.0	95:5
Q10	18.0	2.0	80.0	20.0	90:10
Q20	17.6	4.4	78.0	22.0	80:20

2.4. Electrode Preparation

The porous carbon electrodes used in this study were prepared from a slurry containing activated carbon powder (YEC-8A, 80%, Fuzhou Yihuan Carbon Co), carbon black conductive additive (10%) and polyvinylidine fluoride (PVDF) binder (10%), in *N*-methylpyrrolidone (NMP). The slurry was coated onto a graphite foil current collector (99% Purity, Gee Graphite Ltd) and baked in a vacuum oven at 80℃ for 12 h to evaporate the solvent (Figure S3). The prepared electrodes had an approximate area of 10 mm × 10 mm and had active masses of between 0.01 g and 0.04 g.

2.5. Membrane Characterization

Surface and cross-sectional morphologies of the membranes and electrodes were provided by scanning electron microscopy (SEM) images. SEM images were obtained using an FEI Quanta 250 ESEM instrument. Prior to imaging all membrane samples were sputtered with platinum coating to add conductivity and image resolution. Membrane thicknesses were determined using ImageJ software, taking the average of three measurements over the membrane cross-section. Atomic force microscopy (AFM) topography images were gathered using a Bruker Multimode 8 microscope in tapping mode. Images were analyzed using the Nanoscope Analysis 1.9 software and surface roughness, R_a, was calculated as an average over a 10 μm x 10 μm image.

^{1}H nuclear magnetic resonance (NMR) spectra were obtained using a 400 MHz Bruker Avance III spectrometer. Chemical shifts are given in ppm relative to tetramethylsilane (0 ppm). All spectra were obtained in DMSO-d_6 and referenced to the residual solvent peak (2.500 ppm). Fourier-transform infrared

(FTIR) spectra were recorded using a Bruker Alpha-P ATR-FTIR spectrometer. Elemental analysis was conducted using a dry combustion method of membrane samples, performed with a CHN-elemental analyzer equipped with a halide titrator. Prior to NMR, FTIR and elemental analysis membrane samples were dried under vacuum (~10 mbar) for 24 hours to remove any solvent and unreacted reagent traces.

The structural stability of the polymer blend membranes was tested by immersion of the membranes in the electrolyte utilized during this study (200 mg L^{-1} NaCl in water). In brief, membrane pieces (1 cm width × 3 cm length) were cut and immersed into the electrolyte for a period of 14 days. The weights of dry membrane pieces were recorded before and after immersion and the percentage weight loss in the electrolyte was calculated by:

$$Weight\ Loss\ in\ Electrolyte\ (\%) = \frac{m_{\mathrm{d,before}} - m_{\mathrm{d,after}}}{m_{\mathrm{d,before}}} \times 100\% \quad (1)$$

Ion-exchange capacity (IEC) of the AEMs was determined in triplicate using Mohr's method.[32] Membrane pieces (chloride form) were dried in a vacuum desiccator for 24 h and the dry mass of the pieces was recorded. The pieces were subsequently submerged in KNO_3 aqueous solution (40 mL, 1 M) for 24 h to allow chloride ions to fully exchange into the solution. The membranes pieces were washed with DI water which was mixed with the solution. Five drops of K_2CrO_4 indicator were added to the analyte and titrated against $AgNO_3$ (0.01 M). After all chloride ions had precipitated to form a white precipitate of silver chloride (AgCl), excess Ag^+ ions proceeded to form a dark red silver chromate precipitate (Ag_2CrO_4); signifying the end-point of the titration.[33] The IEC (mmol g^{-1}) of the membranes was subsequently determined by:

$$IEC\ (mmol\ g^{-1}) = \frac{C_{\mathrm{Ag}} V_{\mathrm{S}}}{m_{\mathrm{d}}} \quad (2)$$

where c_{Ag} is the concentration of silver ions in $AgNO_3$, V_S is the titration volume of $AgNO_3$ and m_d is the dry mass of the membrane.

The quaternization degree (QD) was estimated by comparison of the experimental (IEC_{Exp}) and maximum theoretical ion-exchange capacity (IEC_{Theory}) given by:

$$QD\ (\%) = \frac{IEC_{Exp}}{IEC_{Theory}} \times 100\% \quad (3)$$

where (IEC_{Theory}) is derived from the mass percentage of counter-ions in the membrane as determined by elemental analysis. This is given by:

$$IEC_{Theory}(mmol\ g^{-1}) = \frac{Iodide\ Content\ (\%) \times 1000}{M_I \times 100\%} \quad (4)$$

where M_I is the molar mass of iodide ion (126.9 g mol^{-1}).

Permselectivity measurements were determined from chronopotentiometric curves. The membranes were conditioned by immersion into 0.1 M NaCl solution in DI water for 24 h. The membrane was fixed in a sandwich setup with a circular area of 0.19 cm^2 (Figure S1). Platinum mesh electrodes (1 cm × 3 cm) were used as working/counter electrodes and Ag/AgCl were used as reference/sensing electrodes. Both beakers contained equimolar NaCl solution (0.1 M, 50 mL) and were stirred continuously throughout the experiment.

Chronopotentiometry measurements were carried out with a potentiostat (Autolab, Metrohm) in the galvanostatic mode using an overlimiting current of 10 mA. The transition time, τ was determined by the inflection point of the chronopotentiometry curve and substituted into the modified Sand equation to calculate the permselectivity, P given by:

$$P = \frac{|z|FD^{0.5}\pi^{0.5}C}{2\,(1-t_i)\frac{I}{A}\tau^{0.5}} \quad (5)$$

where $|z|$ is the absolute valence of the chloride ion, F is the Faraday constant (96 485 C mol^{-1}), D is the diffusion coefficient (1.48 x 10^{-5} cm^2 s^{-1}), t_i is the transport number (0.61) of the chloride ion in 0.1 M NaCl, I is the applied current (10 mA) and A is the exposed area (0.19 cm^2).[34] The values were calculated as an average of three membrane pieces.

Membrane area resistance values were obtained using the sandwich setup depicted in Figure S1 combined with electrochemical impedance spectroscopy (EIS), with equimolar NaCl (1 M, 50 mL) in each beaker. The measurements were carried out using a potentiostat (Metrohm, Autolab) integrated with frequency response analyser (FRA32M). Platinum mesh electrodes were again used as the working/counter electrodes, and Ag/AgCl electrodes as the reference/sensing electrodes. Impedance measurements were carried out over 50 scans using an AC signal of 0.1 mA and within a frequency range of 1 mHz to 1 kHz.[35] The resistance of the membrane immersed in 1 M NaCl solution (R_{MS}) was obtained as the impedance of the system. The value was calculated using equivalent circuit fitting (Figure S2) of Nyquist plots (real v. imaginary impedance) over the specified frequency range. These resistance values were corrected by the resistance of the solution only (R_S) using a cell with no membrane separating the two solution compartments. The area resistance (R_A) values of the membranes were subsequently calculated by multiplying by the exposed membrane area, A:

$$R_A = (R_{MS} - R_S)A \quad (6)$$

The water contact angle was measured at room temperature in air using a Kruss Drop Shape Analyser (DSA 100 Instrument). Membrane samples were dried in a vacuum desiccator for 24 h prior to the measurements. Droplets were formed on the membrane surface using DI water with a droplet volume of 1.5 μL. The contact angles are reported as an average of three droplets.

Water uptake and linear swelling ratio measurements were determined in triplicate in the chloride form of the membrane. All membrane pieces were submerged in DI water for 24 h and the wet mass (m_w) and length (L_W) were recorded. The samples were dried in a vacuum desiccator for 24 h and the dry mass (m_d) and length (L_d) were recorded. The water uptake and linear swelling ratio as a percentage were determined by the following equations:

$$WU\ (\%) = \frac{m_w - m_d}{m_d} \times 100\% \quad (7)$$

$$LSR\ (\%) = \frac{L_w - L_d}{L_d} \times 100\% \quad (8)$$

2.6. MCDI Desalination Tests

All prepared membranes were used as AEMs in the MCDI cell. The MCDI cell comprises two Perspex end-plates, two porous carbon electrodes coated onto graphite current collectors and the AEM covering the anode. The two electrodes were separated by an acrylic spacer (width = 2 mm) to open up a flow channel and prevent short-circuiting. A schematic of the asymmetric MCDI cell, including cell dimensions, is depicted in Figure S4.

MCDI desalination experiments were carried out on a bench-scale flow-between system as depicted in Figure 2. Membranes were conditioned in electrolyte (NaCl, 200 mg L^{-1}) for 24 h prior to desalination tests. All desalination tests were performed in batch-mode at T = 25°C whereby the effluent stream was recycled back into the feed reservoir. 60 mL of feed salt solution (200 mg L^{-1}) was pumped continuously through the system using a peristaltic pump (VWR) at a flow rate of 5 mL min^{-1}. Voltages of 1.2 and 0.0 V were used for the adsorption and desorption cycles respectively, with each cycle lasting for 1 h. Systems were then recycled using 2h adsorption (1.2 V)/desorption (0.0 V) cycles, to confirm stability of the MCDI system over an extended time period (+30 h). Cell voltages were applied using a potentiostat (Metrohm, Autolab) and desalination was measured by a conductivity meter (Seven Excellence, Mettler Toledo) in the feed

reservoir. Duplicate measurements were taken for all membrane designations and conversion from conductivity (µS cm^{-1}) to salt concentration (mg L^{-1}) was done by a calibration plot (Figure S5).

The desalination performance of the system was evaluated by the salt adsorption capacity (SAC), charge efficiency (Λ) and salt adsorption rate (SAR). The energy normalized to salt adsorption (ENAS) is an important parameter defining the amount of salt removed per unit energy. These metrics are defined by:

$$SAC\ (mg\ g^{-1}) = \frac{(C_0 - C_{eff})V_s}{m_e} \quad (9)$$

$$\Lambda\ (\%) = \frac{(C_0 - C_{eff})V_s F}{MQ} \times 100\% \quad (10)$$

$$SAR\ (mg\ g^{-1}\ min^{-1}) = \frac{SAC}{t} \quad (11)$$

$$ENAS\ (\mu mol\ J^{-1}) = \frac{(C_0 - C_{eff})V_s}{ME_{ads}} \quad where\ E_{ads} = V \int Idt \quad (12)$$

where C_0 , C_{eff} are the initial and effluent concentrations (mg L^{-1}) respectively, V_s (L) is the volume of the feed solution, m_e is the combined electrode mass (g), M is the molar mass of NaCl (58.5 g mol^{-1}), F is the Faraday constant (96485 C mol^{-1}) and t (minutes) is the adsorption time. Q is the total charge (C) supplied during the charging process, calculated as the time integral of the current $\int Idt$. E_{ads} is the energy expended during the adsorption step in constant voltage MCDI operation. All values were taken as an average of three cycles when the systems had reached a dynamic equilibrium (when the salt adsorption in one half of the cycle was equal to the salt desorption in the subsequent half cycle).

3. Results & Discussion

3.1 Membrane Structure and Morphology

The surface morphologies of the polymer blend membranes were characterized by SEM and AFM imaging. As observed in Figure 3 (a–d), the number of surface features increases with the amount of PEI loading. During sonication of the casting solution, PEI is dissolved into the PBI/DMAc casting solution. The vigorous mixing of the dope solution creates entanglement of PEI within PBI chains, the extent of which is dependent on the PEI wt% in the dope solution. Solution casting of membranes and immediate annealing at 60 °C for 24 h resulted in fixed PEI chains confined in the aromatic PBI backbone; forming a tight and densely packed membrane layer (Cross-sectional SEM, Figures 3e–h). Due to the abundance of nitrogen containing functional groups in both polymers; PEI would be entrapped within the blend structure during

mixing via hydrogen bonding interactions. Furthermore, the blend structure benefited from ion-stabilization after modification by methyl ($–CH_3$) groups during the quaternization step. The presence of opposing quaternary ammonium (positive) and chloride (negative) species in the backbone of the AEMs created additional electrostatic interactions, resulting in a stable blend network. Similar polymer blends have been reported; whereby PBI/PIM-1 composites were ion-stabilized by amine protonation via treatment with HCl.[36]

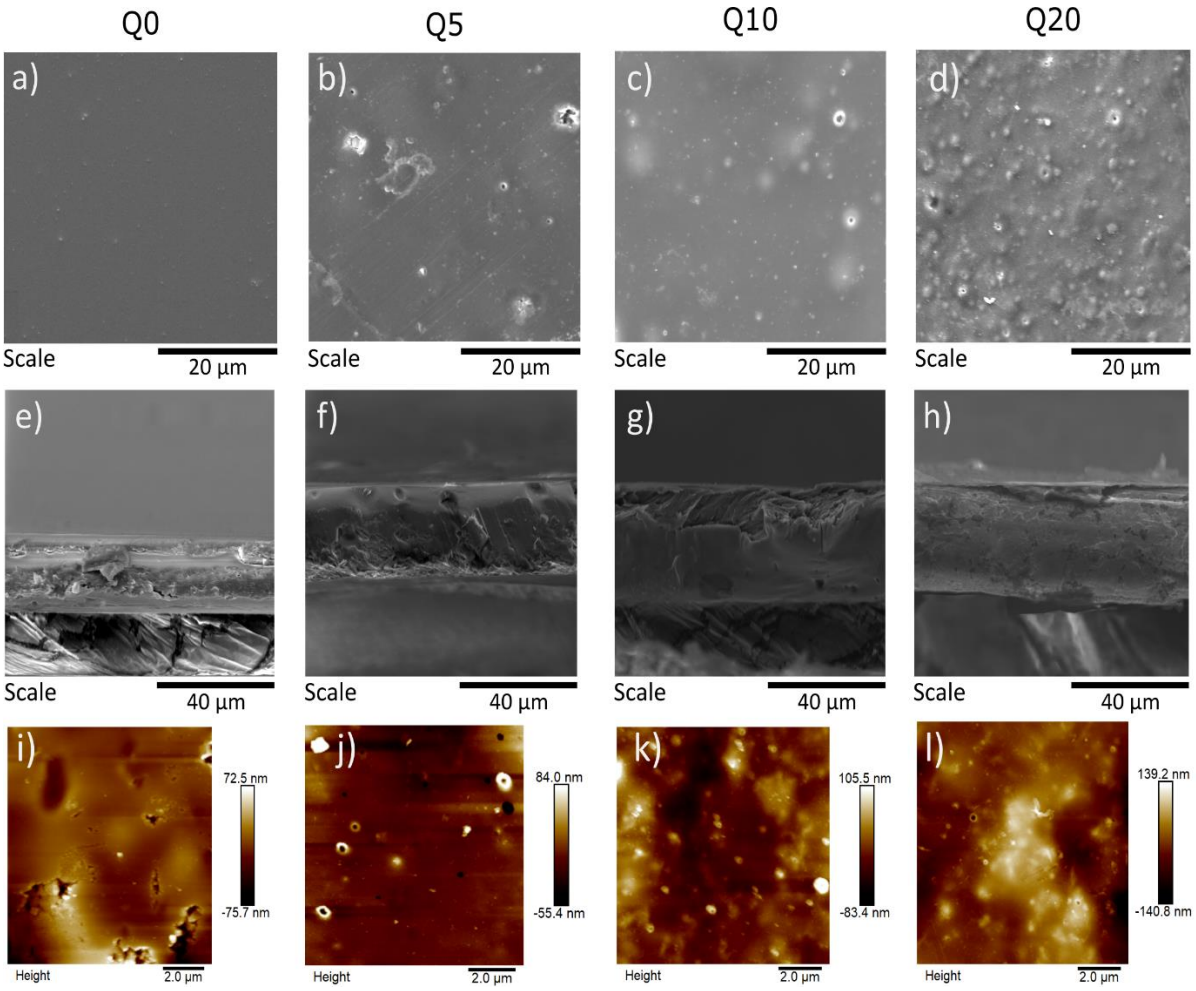

Figure 3. SEM images displaying surface (a–d) and cross-sectional (e–h) morphologies of the membranes, and AFM images (i–l) revealing the roughness of all membranes.

Table 2 lists structural properties of fabricated membranes. Thickness and roughness parameters were determined via ImageJ and Nanoscope software, respectively. All polymer blend membranes showed an increase in thickness compared to the Q0 (PBI only) membrane. This is attributed to an increased mass loading of PEI into the original casting solution, given that an identical air gap (200 µm) was used to cast all membranes. AFM images show a gradual increase in surface roughness for membranes Q0 to Q20. The

average arithmetic roughness values (R_a) were calculated over a 10 × 10 μm AFM image. The increasing surface roughness has potential to increase the hydrophilicity of membranes according to Wenzel theory; attributed to an increase in the solid/liquid contact area on the membrane surface. The PEI domains embedded within the PBI matrix create a rougher surface with undulations, increasing the surface area compared to the pristine Q0 membrane. This effect, combined with the hydrophilic nature of PEI compared to hydrophobic PBI, can create a surface with enhanced wetting properties.[37] This could improve the initial uptake of chloride ions and subsequent transport through the AEMs. The SEM and AFM images suggested successful embedding of PEI within the PBI backbone. Further, all membranes showed good structural stability after immersion tests in the studied electrolyte (NaCl, 200 mg L^{-1}) after a period of 14 days; with all membranes retaining +95% of their original mass after immersion. This inferred that the membranes retained excellent confinement of PEI within the blended matrix and stability of the membrane structure after extended exposure to saline water.

Table 2. Morphological and dimensional properties of prepared membranes.

Membrane	Thickness (μm)	R_a (nm)	Linear Swelling Ratio (%)	Weight Loss in Electrolyte (%)
Q0	29.8 ± 0.4	8.2	7.7 ± 4.2	4.3 ± 1.6
Q5	34.2 ± 0.9	10.8	6.9 ± 0.4	1.9 ± 0.6
Q10	34.6 ± 0.4	20.4	8.3 ± 3.2	1.6 ± 0.8
Q20	36.4 ± 0.8	30.6	11.9 ± 4.2	3.2 ± 1.2

3.2 Membrane Quaternization

Anion-exchange characteristics was imparted to the membranes by chemical modification via a nucleophilic methylation (S_N2) reaction. In PBI, methylation occurs by substitution of methyl groups onto the aromatic nitrogen on the imidazole ring to form imidazolium cationic moieties throughout the PBI backbone.[38] Likewise, PEI contains an abundance of primary, secondary and tertiary amine groups that can undergo quaternization. Figure 4a) displays ^{1}H NMR spectra for all AEMs in DMSO-d_6 solvent. The signals between 7.5–8.5 ppm can be assigned to aromatic protons within the imidazole/imidazolium rings. The characteristic signal showing the N–H proton on the imidazole ring for PBI is found at 13.2 ppm.[39] This signal is no longer distinguishable in any of the quaternized membranes Q5–Q20; indicating that most of the N–H protons in PBI were methyl substituted during alkylation or otherwise deprotonated. For all quaternized membranes a new multiplet signal at 4.1 ppm was observed. This signal is well-known and

corresponds to the methyl protons substituted onto the nitrogen of benzimidazolium.[40] These assignments indicate successful quaternization of the PBI backbone in the AEMs.

Additional ^{1}H NMR signals imply successful PEI incorporation and quaternization. Typical signals at 2.3–3.0 ppm can be observed at different intensities for all of Q5, Q10 and Q20, which are not apparent in the PBI and Q0 membranes. These can be assigned to methylene (–CH_2–) protons in the aliphatic branched PEI chains.[41] Further signals at 0.8–1.2 ppm match well with literature values assigned to quaternized polyethylenimine after alkylation with a methyl group.[42] Further information on the quaternization of membranes was gathered via elemental analysis (Table 3). The iodide content gives the percentage by mass of counter-ion within the membrane after methylation. A higher iodide content indicates a higher level of quaternization and a higher theoretical ion-exchange capacity (Equation 4) of the membranes. Q0 has the lowest iodide content (23%) of all the prepared membranes. The iodide content subsequently increases with increasing PEI content in the blend AEMs. However, only a slight increase was observed upon doubling the mass loading between Q10 (35%) and Q20 (36%). This implied that nitrogen groups became less accessible to quaternization at higher mass loadings of PEI; as PEI domains become shielded by neighboring PBI-PEI groups to a greater extent. Nevertheless, the NMR and elemental analysis data demonstrate that with higher amounts of PEI in the PBI matrix, this can increase the level of counter-ions and the theoretical IEC of the membranes. This should result in increased Cl^{-} removal and salt adsorption capacity when quaternized membranes are used as an AEM in an MCDI system.

Table 3. Elemental compositions of all membranes determined by elemental analysis.

Membrane	Elemental Composition (%)				Maximum Theoretical IEC (mmol g^{-1})
	C	N	H	I	
Q0	51.08	11.40	3.38	23.22	1.83
Q5	44.18	10.08	4.17	31.39	2.47
Q10	42.06	9.98	4.47	35.34	2.77
Q20	41.46	9.76	4.35	35.78	2.82

Figure 4b) displays FTIR spectra of all fabricated membranes and pristine PBI and PEI polymers. A broad transmittance peak can be observed (3000–3500) cm^{-1} for all membranes, corresponding to the N–H stretching on the imidazole rings and primary amine groups in PEI. The peak found at 1620 cm^{-1} can be assigned to the C=N stretch on the imidazole ring. Spectra for Q10 and Q20 membranes display two peaks in the region (2850–2950) cm^{-1}. These peaks are characteristic of aliphatic C–H stretching vibrations and

have been previously reported as due to the addition of a greater number of alkyl groups in a quaternized membrane.[43] Due to the higher loading of PEI, the C–H vibration would become more intense as a result of higher number of methyl substituents after quaternization. The complementary NMR, elemental analysis and FTIR data indicate successful quaternization of PBI and PEI, and these data suggest that quaternized PEI can introduce additional counter-ions into the membrane.

3.3 Hydrophilicity of Membranes

Hydrophilicity and wettability properties of the AEMs were determined by analysis of the contact angles and water uptake of membrane pieces (Figure 4c). Good hydration properties of membranes can positively affect ion transport; however, excessive swelling can hinder certain electrochemical properties of the membranes such as permselectivity.[44] A lower contact angle is representative of a membrane's hydrophilic nature due to a reduction in the surface tension between the water/membrane interface.[45] Q0 and Q5 displayed the most hydrophobic properties with contact angles of 62° and 63°, respectively. This hydrophobicity is reinforced by water uptake values of 19% (Q0) and 16% (Q5). Usually, the introduction of hydrophilic PEI domains into hydrophobic PBI is expected to decrease contact angle whilst increasing water uptake. These results suggest that the addition of PEI in small quantities (5 wt%) had no marked effect on the hydrophilic properties of the blend membrane. Increasing the mass loading of PEI resulted in a discernible drop in the contact angle to 53° (Q10) and 50° (Q20) and a simultaneous increase in water uptake of 26% (Q10) and 34% (Q20). Promisingly, these values of water uptake match closely to the typical values of Neosepta-AMX (25–30%) and Fumasep-FAA (15–30%) ion-exchange membranes.[46] Therefore, it is reasonable to deduce that water permeability for these membranes is not sufficiently high to compromise the membrane performance in MCDI. These values show that increasing the mass loading of PEI can act to modify the wetting properties of the membranes, as water molecules become confined in hydrophilic passages (PEI) in an otherwise hydrophobic (PBI) matrix. This increase in hydrophilicity has the potential to increase hydration and the anion conductivity of the membranes.

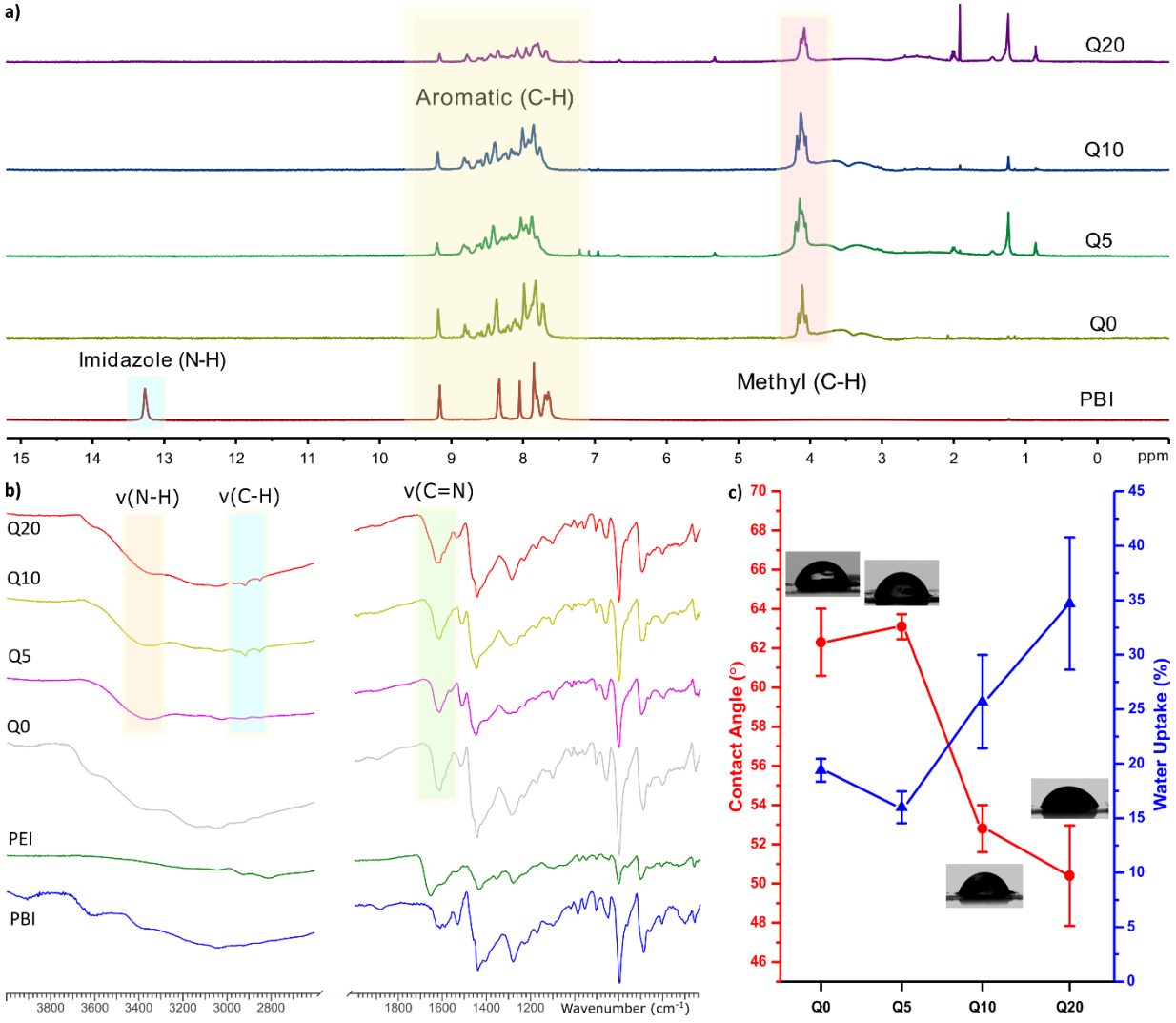

Figure 4. a) ^{1}H NMR spectra for all membranes in DMSO-d_6 (solvent peak DMSO (2.50 ppm) and water (3.30 ppm) are suppressed for these spectra), b) FTIR spectra of pristine polymers and polymer blend membranes, c) Plot displaying contact angles and water uptake of the prepared membranes.

3.3 Electrochemical Properties of Membranes

The ion-exchange capacity (IEC) of membranes is a crucial property; in AEMs, a high IEC will theoretically increase the number of chloride ions removed from saline water and subsequently transported and stored in the porous activated carbon electrodes.[47] The introduction of PEI into PBI should introduce many cationic groups and corresponding counter-ions into the membrane after methylation. Figure 5a) displays experimental and theoretical IEC values for prepared and commercial membranes. Q0 had a relatively low IEC of 1.53 mmol g^{-1}, supporting the aforementioned elemental analysis results with Q0 having the lowest iodide content of all AEMs tested. The IEC of PEI-incorporated membranes Q5, Q10 and Q20 showed

strong improvement, giving high values of 2.27, 2.50 and 2.63 mmol g^{-1}, respectively. The quaternization degree (QD, Equation 3) was determined by direct comparison of experimental and theoretical IEC. Calculated QD values were 84%, 92%, 90% and 93% for membranes Q0, Q5, Q10 and Q20, respectively. QD values were over 90% for all blend membranes, indicative of highly quaternized structures with high concentrations of charge carriers and counter-ions. All prepared PEI-incorporated membranes exhibited higher IEC values than the commercially available and high-performing AMX and FAA AEMs (Figure 5a);[27,46] giving further credence to their application in MCDI. The experimental IEC values justified the incorporation of PEI groups into the PBI matrix: Q5, Q10 and Q20 all displayed superior ion exchange properties to the pristine Q0 membrane. These superior properties can be attributed to the blend membranes containing polymers which were both quaternized, resulting in abundant anion transport pathways throughout the membranes.

Table 4 provides values for the permselectivity and area resistance of the prepared membranes. Permselectivity was used to quanitify the counter-ion (chloride) selectivity of the membranes, which was determined from chronopotentiometric curves (Figure S6). The quaternized blended membranes showed higher permselectivity (Table 4) than did the pristine Q0 membrane, likely the result of the higher volume of fixed cationic groups (quaternary ammonium donated by the PEI polymer) acting to block the transport of sodium co-ions through the membrane. While all quaternized blended AEMs showed higher permselectivity than Q0, the values obtained were less than ideal permselectivity ($P = 1$) due to the increased water uptake of the PEI-containing membranes. Nevertheless, the hydration of the membranes was not so excessive as to sufficiently dilute the high concentration of quaternary ammonium charge carriers and sacrifice membrane permselectivity.[48]

Membrane area resistance is another crucial electrochemical property of ion-exchange membranes. Low area resistance is preferential to improve ion transfer across the electrode/membrane interface, hence increasing the energy efficiency of the MCDI process.[49] All blended membranes showed reduced area resistance compared to Q0 membrane (8.76 Ω cm^2). Q10 (1.99 Ω cm^2) and Q20 (1.46 Ω cm^2) membranes exhibited significant reduction in area resistance, owing to their enhanced hydrophilic properties and IEC. The combination of high IEC, low area resistance and good permselectivity of the highly quaternized blended AEMs pointed to excellent membrane properties for application in MCDI. Area resistance values obtained for Q10 and Q20 were below those of selected commercial IEMs, however permselectivity values were slightly lower than expected values.[46] This is a likely side-effect of the increased water uptake and IEC, introducing small amounts of Na^+ ions into the membrane. Nevertheless, a maximum permselectivity

value of 0.86 was achieved for the Q20 membrane. A good permselectivity is favorable for minimizing co-ion expulsion during MCDI cycling.[50]

Table 4. Permselectivity and area resistance values for the prepared membranes.

Membrane	Permselectivity	Area Resistance (Ω cm^2)
Q0	0.79 ± 0.03	8.76 ± 0.29
Q5	0.83 ± 0.01	5.06 ± 0.23
Q10	0.83 ± 0.03	1.99 ± 0.37
Q20	0.86 ± 0.05	1.46 ± 0.29

3.4. MCDI Desalination Performance

Asymmetric MCDI cells were assembled as depicted in Figure S4, with quaternized AEMs covering the anode only. The electrodes had an approximate area of 1 cm^2 and were separated by a spacer of width 2 mm to open up a flow channel. A flow rate of 5 mL min^{-1} was chosen to provide a sufficient ion residence time for uptake through the membrane/electrode. A constant salt water concentration of 200 mg L^{-1} was chosen for desalination tests; this salt content was previously employed in MCDI studies.[19,51] Both salt adsorption capacity and charge efficiency can be influenced by the feed salt concentration,[21,52] therefore a constant salt concentration was maintained throughout all experiments to isolate the effects of the AEM on the MCDI performance.

Prior to desalination, cyclic voltammetry (CV) responses were recorded for all systems. The voltage was varied between 0.0 V and 1.2 V at a scan rate of 0.2 V s^{-1} and the current response was measured. CVs are displayed in Figure S7 and are indicative of the capacitive behavior of all MCDI systems, with no observed oxidation or reduction peaks at any voltage. Figure 5b) shows the conductivity profile and regenerative behavior of the MCDI system using the Q20 membrane. During each adsorption/desorption cycle a conductivity drop is observed during the charging step (1.2 V), followed by an increase in conductivity during short-circuiting (0.0 V). These results are consistent with regeneration profiles found in batch-mode MCDI configurations,[51,53,54] indicating that membranes can maintain the characteristic desalination performance over repeated cycles. Analogous behavior was observed for the Q0, Q5 and Q10 membranes; shown in Figure S10–S12, respectively. The systems tended to reach dynamic equilibrium after around four adsorption/desorption cycles. To confirm cycling stability over extended periods, the MCDI systems were subjected to longer (2h) adsorption/desorption cycles. This was done immediately after an initial

cycling of 1h adsorption/desorption cycles (up to 50h total). The profiles depicted in Figures S13 and S14 show consistent cycling and conductivity profiles over this period, demonstrating that AEMs can maintain desalination performance over long term MCDI operation and for cycles of longer duration.

SAC and charge efficiency values for all systems are shown in Figure 5d); all MCDI systems show drastic improvement in SAC compared to CDI without membranes (4.2 mg g^{-1}). Additionally, all quaternized polymer blended membranes displayed higher salt adsorption capacity than the Q0 membrane without PEI polymer (9.4 mg g^{-1}). The salt adsorption capacity increased with increasing PEI content giving values of 10.6, 11.6 and 13.2 mg g^{-1} for Q5, Q10 and Q20, respectively. Charge efficiency values showed strong improvement compared with conventional CDI (27.7%). Again, charge efficiency values showed an increase as the PEI mass loading of the membrane increased. The pristine Q0 membrane MCDI system exhibited modest charge efficiency (40.5%), whist the quaternized blend AEMs returned values of 50.0%, 55.7% and 67.9%, respectively.

Additionally, salt adsorption rate (SAR) and energy normalized to adsorbed salt results are displayed in Table 5. The lower resistance to ion transfer, combined with abundant fixed charged carriers, increased the salt adsorption rate (SAR) of the MCDI systems. The measured SAR values were 0.16, 0.18, 0.19 and 0.22 mg g^{-1} min^{-1} for Q0, Q5, Q10 and Q20 membranes, respectively. This gradual increase further highlights the positive influence that quaternized PEI domains can have on the rate of ion transport into the electrodes. Likewise, ENAS is a crucial performance metric, relating the quantity of salt removed per unit energy supplied during charging. This value increased consistently with increasing PEI content. The Q20 membrane (5.87 µmol J^{-1}) displayed more than double the value of the CDI (2.39 µmol J^{-1}) system, indicating a system with superior energy efficiency. The highest ENAS value (Q20 membrane) was comparable to some literature values obtained for a symmetric cell employing both a commercial AEM and CEM,[49] however was slightly lower than for polyelectrolyte-coated activated carbon electrodes.[55]

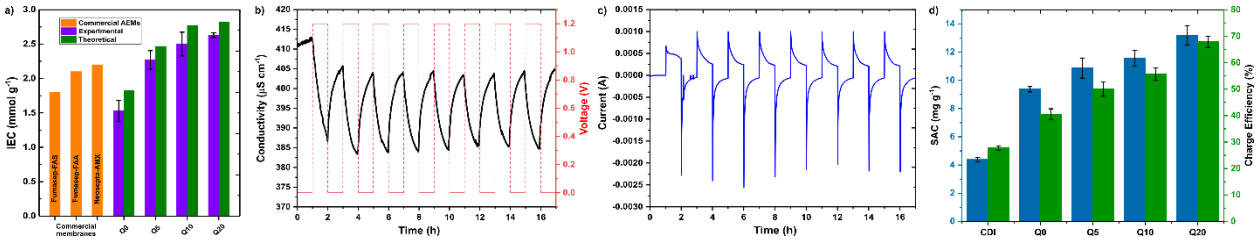

Figure 5. a) Ion-exchange capacity (IEC) values of prepared and commercial AEMs. Theoretical IEC derived from the iodide content of the membranes in the elemental analysis (Equation 4), b) Repeated adsorption/desorption cycles over repeated cycles using the Q20 anion-exchange membrane, c) current response over time using the Q20 anion-exchange membrane, d) Graph displaying salt adsorption capacity

(SAC) and charge efficiency values for conventional CDI and all membranes in the asymmetric MCDI system.

The results validated the use of quaternized polymer blends as AEMs in MCDI. The SAC and SAR values obtained for each MCDI system scaled with increasing IEC of the membranes following Q0 < Q5 < Q10 < Q20. The high IEC and permselectivity of the membranes selectively permitted more counter-ions (chloride) to transport into the electrode pores during adsorption, due to the high volume of cationic ammonium charge carriers in the membrane backbone. Further, the significantly reduced area resistance of the quaternized blended AEMs was beneficial to co-ion effects. During desorption, expelled co-ions were blocked from entering the spacer channel whilst counter-ions were readily desorbed across the membranes with low ionic resistance. This also explains the increase in charge efficiency and ENAS in the MCDI systems; corresponding to a decrease in the area resistance between Q0 and Q20 AEMs.

Table 5. Salt adsorption rate (SAR) and energy normalized to adsorbed salt (ENAS) values for all systems.

(M)CDI System	SAR (mg g^{-1} min^{-1})	ENAS (µmol J^{-1})
CDI	0.07 ± 0.00	2.39 ± 0.06
Q0	0.16 ± 0.00	3.52 ± 0.19
Q5	0.18 ± 0.01	4.30 ± 0.20
Q10	0.19 ± 0.01	4.84 ± 0.20
Q20	0.22 ± 0.01	5.87 ± 0.19

The improvement of all MCDI systems compared with CDI can be rationalized by co-ion effects. Membranes with high permselectivity (MCDI) result in an accumulation of co-ions in the macropores of the carbon electrodes, as the transport of sodium ions back into the spacer channel (co-ion expulsion) is blocked. This draws across more counter-ions to maintain electroneutrality in the macropore region, increasing the salt adsorption during subsequent adsorption cycles.[56] These co-ion effects elucidate the significant increase in SAC (3.1 times higher) and charge efficiency (2.5 times higher) of MCDI with the Q20 membrane compared with conventional CDI. Owing to the higher IEC, reduced area resistance and higher permselectivity, the use of the Q20 (SAC 13.2 mg g^{-1}) membrane improved the desalination performance by a factor of 40% compared with the Q0 membrane without PEI (9.4 mg g^{-1}). Furthermore, the fabricated membranes outperformed similar MCDI systems in the literature as shown in Table S1. The application of quaternized blended AEMs has been shown to positively affect desalination performance in MCDI, even with an unprotected cathode. The superior performance of all blended AEMs compared to

Q0 vindicates the incorporation of quaternized PEI. This study has systematically investigated the effect of quaternized PBI/PEI membranes on the desalination performance of MCDI. In future works, focus will be placed on optimization of factors such as membrane structure, polymer blend interactions, dope solution composition and quaternization conditions. This optimization will further improve the salt removal and energy efficiency of the systems and give insight into the feasibility of the membranes for industrial MCDI application.

4. Conclusions

In this work, AEMs for MCDI were fabricated based on quaternized PBI/PEI polymer blends. The membranes were prepared by a phase inversion process followed by heat treatment and quaternization by methylation. The highest performing Q20 membrane exhibited excellent electrochemical properties such as high IEC (2.6 mmol g^{-1}), good permselectivity (0.86) and low area resistance (1.46 Ω cm^2). We attributed these properties to the abundance of anion-selective quaternary ammonium groups introduced in the PBI/PEI backbone. Quaternized AEMs demonstrated superior performance to the performance of both CDI (without membranes) and the pristine Q0 membrane. The employment of the Q20 membrane as AEM provided a large increase in SAC (13.2 mg g^{-1}, 3.1 times higher), charge efficiency (67.9%, 2.5 times higher), SAR (0.22 mg g^{-1} min^{-1}, 3.1 times higher) and ENAS (5.87 µmol J^{-1}, 2.4 times higher), compared to CDI without an AEM. Overall, this study outlines a simple preparation method for high performance AEMs for MCDI. The utilization of quaternized polymer blends as AEMs in MCDI has potential to enhance membrane properties and improve desalination performance. These factors could pave the way for greater practical realization of MCDI for industrial desalination of water supplies.

Notes

The authors declare no competing financial interest.

Supporting Information

File includes experimental setup for electrochemical measurements, equivalent circuit model, SEM images of activated carbon electrodes, asymmetric MCDI schematic, calibration data, EDX plots, CV curves, MCDI profiles of all membranes and table of comparisons to other MCDI literature.

Acknowledgements

The authors would like to thank Martin Jennings (Dept. of Chemistry, University of Manchester) for elemental analysis measurements. The authors acknowledge the UK's Engineering and Physical Sciences Research Council (EPSRC) under grant code EP/L01548X/1 for funding Robert McNair's doctoral studies through the University of Manchester's Graphene NOWNANO CDT account. Further equipment funding via EPSRC grants EP/S019367/1 and EP/P025021/1 to the Royce Institute is also gratefully acknowledged. The graphical abstract, Figures 1 and 2 were created by Xavier Pita, scientific illustrator at King Abdullah University of Science and Technology (KAUST). The research reported in this publication was supported by funding from KAUST.

References

(1) Mekonnen, M. M.; Hoekstra, A. Y. Sustainability: Four Billion People Facing Severe Water Scarcity. *Sci. Adv.* **2016**, *2* (2), e1500323.

(2) Elimelech, M.; Phillip, W. A. The Future of Seawater Desalination: Energy, Technology, and the Environment. *Science* **2011**, *333* (6043), 712-717.

(3) Qasim, M.; Badrelzaman, M.; Darwish, N. N.; Darwish, N. A.; Hilal, N. Reverse Osmosis Desalination: A State-of-the-Art Review. *Desalination* **2019**, *459*, 59-104.

(4) Wang, L.; Dykstra, J. E.; Lin, S. Energy Efficiency of Capacitive Deionization. *Environ. Sci. Technol.* **2019**, *53* (7), 3366-3378.

(5) Choi, J.; Oh, Y.; Chae, S.; Hong, S. Membrane Capacitive Deionization-Reverse Electrodialysis Hybrid System for Improving Energy Efficiency of Reverse Osmosis Seawater Desalination. *Desalination* **2019**, *462*, 19-28.

(6) Biesheuvel, P. M.; van der Wal, A. Membrane Capacitive Deionization. *J. Membr. Sci.* **2010**, *346* (2), 256-262.

(7) Wang, G.; Pan, C.; Wang, L.; Dong, Q.; Yu, C.; Zhao, Z.; Qiu, J. Activated Carbon Nanofiber Webs Made by Electrospinning for Capacitive Deionization. *Electrochim. Acta* **2012**, *69*, 65-70.

(8) Xu, P.; Drewes, J. E.; Heil, D.; Wang, G. Treatment of Brackish Produced Water Using Carbon Aerogel-Based Capacitive Deionization Technology. *Water Res.* **2008**, *42* (10-11), 2605-2617.

(9) Li, H.; Gao, Y.; Pan, L.; Zhang, Y.; Chen, Y.; Sun, Z. Electrosorptive Desalination by Carbon Nanotubes and Nanofibres Electrodes and Ion-Exchange Membranes. *Water Res.* **2008**, *42* (20), 4923-4928.

(10) Liu, P.; Yan, T.; Shi, L.; Park, H. S.; Chen, X.; Zhao, Z.; Zhang, D. Graphene-Based Materials for Capacitive Deionization. *J. Mater. Chem. A*. **2017,** *5* (27), 13907-13943.

(11) Jia, F.; Sun, K.; Yang, B.; Zhang, X.; Wang, Q.; Song, S. Defect-Rich Molybdenum Disulfide as Electrode for Enhanced Capacitive Deionization from Water. *Desalination* **2018**, *446*, 21-30.

(12) Srimuk, P.; Kaasik, F.; Krüner, B.; Tolosa, A.; Fleischmann, S.; Jäckel, N.; Tekeli, M. C.; Aslan, M.; Suss, M. E.; Presser, V. MXene as a Novel Intercalation-Type Pseudocapacitive Cathode and Anode for Capacitive Deionization. *J. Mater. Chem. A* **2016**, *4* (47), 18265-18271.

(13) Kim, K.; Cotty, S.; Elbert, J.; Chen, R.; Hou, C. H.; Su, X. Asymmetric Redox-Polymer Interfaces for Electrochemical Reactive Separations: Synergistic Capture and Conversion of Arsenic. *Adv. Mater.* **2020**, *32*, 1906877-1906885.

(14) Su, X.; Tan, K. J.; Elbert, J.; Rüttiger, C.; Gallei, M.; Jamison, T. F.; Hatton, T. A. Asymmetric Faradaic Systems for Selective Electrochemical Separations. *Energy Environ. Sci.* **2017**, *10*, 1272-1283.

(15) Biesheuvel, P. M.; Zhao, R.; Porada, S.; van der Wal, A. Theory of Membrane Capacitive Deionization Including the Effect of the Electrode Pore Space. *J. Colloid Interface Sci.* **2011**, *360* (1), 239-248.

(16) Zhang, C.; He, D.; Ma, J.; Tang, W.; Waite, T. D. Faradaic Reactions in Capacitive Deionization (CDI) - Problems and Possibilities: A Review. *Water Res*. **2018,** *128*, 314-330.

(17) Zhao, R.; Porada, S.; Biesheuvel, P. M.; Van der Wal, A. Energy Consumption in Membrane Capacitive Deionization for Different Water Recoveries and Flow Rates, and Comparison with Reverse Osmosis. *Desalination* **2013**, *330*, 35-41.

(18) Duan, F.; Du, X.; Li, Y.; Cao, H.; Zhang, Y. Desalination Stability of Capacitive Deionization Using Ordered Mesoporous Carbon: Effect of Oxygen-Containing Surface Groups and Pore Properties. *Desalination* **2015**, *376*, 17-24.

(19) Chang, J.; Tang, K.; Cao, H.; Zhao, Z.; Su, C.; Li, Y.; Duan, F.; Sheng, Y. Application of Anion Exchange Membrane and the Effect of Its Properties on Asymmetric Membrane Capacitive Deionization. *Sep. Purif. Technol.* **2018**, *207*, 387-395.

(20) Haq, O. ul; Choi, J. H.; Lee, Y. S. Anion-Exchange Membrane for Membrane Capacitive Deionization Prepared via Pore-Filling Polymerization in a Porous Polyethylene Supporting Membrane. *React. Funct. Polym.* **2018**, *132*, 36-42.

(21) Tian, G.; Liu, L.; Meng, Q.; Cao, B. Preparation and Characterization of Cross-Linked Quaternised Polyvinyl Alcohol Membrane/Activated Carbon Composite Electrode for Membrane Capacitive Deionization. *Desalination* **2014**, *354*, 107-115.

(22) Zhang, Y.; Zou, L.; Wimalasiri, Y.; Lee, J. Y.; Chun, Y. Reduced Graphene Oxide/Polyaniline Conductive Anion Exchange Membranes in Capacitive Deionisation Process. *Electrochim. Acta* **2015**, *182*, 383-390.

(23) Xu, C.; Scott, K.; Li, Q.; Yang, J.; Wu, X. A Quaternary Polybenzimidazole Membrane for Intermediate Temperature Polymer Electrolyte Membrane Fuel Cells. *Fuel Cells* **2013**, *13* (2), 118-125.

(24) Zhu, J.; Zhang, Y.; Tian, M.; Liu, J. Fabrication of a Mixed Matrix Membrane with in Situ Synthesized Quaternized Polyethylenimine Nanoparticles for Dye Purification and Reuse. *ACS Sustain. Chem. Eng.* **2015**, *3* (4), 690-701.

(25) Liu, Y.; Pan, L.; Xu, X.; Lu, T.; Sun, Z.; Chua, D. H. C. Enhanced Desalination Efficiency in Modified Membrane Capacitive Deionization by Introducing Ion-Exchange Polymers in Carbon Nanotubes Electrodes. *Electrochim. Acta* **2014**, *130*, 619-624.

(26) Fan, H.; Yip, N. Y. Elucidating Conductivity-Permselectivity Tradeoffs in Electrodialysis and Reverse Electrodialysis by Structure-Property Analysis of Ion-Exchange Membranes. *J. Membr. Sci.* **2019**, *573*, 668-681.

(27) Ran, J.; Wu, L.; He, Y.; Yang, Z.; Wang, Y.; Jiang, C.; Ge, L.; Bakangura, E.; Xu, T. Ion Exchange Membranes: New Developments and Applications. *J. Membr. Sci*. **2017**, *522*, 267-291.

(28) Asadi Tashvigh, A.; Chung, T. S. Facile Fabrication of Solvent Resistant Thin Film Composite Membranes by Interfacial Crosslinking Reaction between Polyethylenimine and Dibromo-p-Xylene on Polybenzimidazole Substrates. *J. Membr. Sci.* **2018**, *560*, 115-124.

(29) Hu, L.; Gao, L.; Zhang, C.; Yan, X.; Jiang, X.; Zheng, W.; Ruan, X.; Wu, X.; Yu, G.; He, G. "Fishnet-like" Ion-Selective Nanochannels in Advanced Membranes for Flow Batteries. *J. Mater. Chem. A* **2019**, *7* (37), 21112-21119.

(30) Carmona-Orbezo, A.; Le Fevre, L. W.; Dryfe, R. A. W. Performance Optimization of Carbon Electrodes for Capacitive Deionization by Potentiostatic Analysis. *Electrochim. Acta* **2019**, *325*, 134898.

(31) Cseri, L.; Baugh, J.; Alabi, A.; AlHajaj, A.; Zou, L.; Dryfe, R. A. W.; Budd, P. M.; Szekely, G. Graphene Oxide-Polybenzimidazolium Nanocomposite Anion Exchange Membranes for Electrodialysis. *J. Mater. Chem. A* **2018**, *6* (48), 24728-24739.

(32) Doughty, H. W. Mohr's Method for the Determination of Silver and Halogens in Other than Neutral Solutions. *J. Am. Chem. Soc.* **1924**, *46* (12), 2707-2709.

(33) Lee, K. H.; Cho, D. H.; Kim, Y. M.; Moon, S. J.; Seong, J. G.; Shin, D. W.; Sohn, J. Y.; Kim, J. F.; Lee, Y. M. Highly Conductive and Durable Poly(Arylene Ether Sulfone) Anion Exchange Membrane with End-Group Cross-Linking. *Energy Environ. Sci.* **2017**, *10* (1), 275-285.

(34) Pismenskaia, N.; Sistat, P.; Huguet, P.; Nikonenko, V.; Pourcelly, G. Chronopotentiometry Applied to the Study of Ion Transfer through Anion Exchange Membranes. *J. Membr. Sci.* **2004**, *228* (1), 65-76.

(35) Abdu, S.; Martí-Calatayud, M. C.; Wong, J. E.; García-Gabaldón, M.; Wessling, M. Layer-by-Layer Modification of Cation Exchange Membranes Controls Ion Selectivity and Water Splitting. *ACS Appl. Mater. Interfaces* **2014**, *6* (3), 1843-1854.

(36) Ignacz, G.; Fei, F.; Szekely, G. Ion-Stabilized Membranes for Demanding Environments Fabricated from Polybenzimidazole and Its Blends with Polymers of Intrinsic Microporosity. *ACS Appl. Nano Mater.* **2018**, *1* (11), 6349-6356.

(37) Moazzam, P.; Tavassoli, H.; Razmjou, A.; Warkiani, M. E.; Asadnia, M. Mist Harvesting Using Bioinspired Polydopamine Coating and Microfabrication Technology. *Desalination* **2018**, *429*, 111-118.

(38) Jheng, L. C.; Hsu, S. L. C.; Lin, B. Y.; Hsu, Y. L. Quaternized Polybenzimidazoles with Imidazolium Cation Moieties for Anion Exchange Membrane Fuel Cells. *J. Membr. Sci.* **2014**, *460*, 160-170.

(39) Chuang, S. W.; Hsu, S. L. C. Synthesis and Properties of a New Fluorine-Containing Polybenzimidazole for High-Temperature Fuel-Cell Applications. *J. Polym. Sci., Part A: Polym. Chem.* **2006**, *44* (15), 4508-4513.

(40) Henkensmeier, D.; Kim, H. J.; Lee, H. J.; Lee, D. H.; Oh, I. H.; Hong, S. A.; Nam, S. W.; Lim, T. H. Polybenzimidazolium-Based Solid Electrolytes. *Macromol. Mater. Eng.* **2011**, *296* (10), 899-908.

(41) Lan, T.; Guo, Q.; Shen, X. Polyethyleneimine and Quaternized Ammonium Polyethyleneimine: The Versatile Materials for Combating Bacteria and Biofilms. *J. Biomater. Sci., Polym. Ed.* **2019**, *30* (14), 1243-1259.

(42) Yew, P. Y. M.; Chee, P. L.; Cally, O.; Zhang, K.; Liow, S. S.; Loh, X. J. Quarternized Short Polyethylenimine Shows Good Activity against Drug-Resistant Bacteria. *Macromol. Mater. Eng.* **2017**, *302* (9), 1700186-1700197.

(43) Xia, Z.; Yuan, S.; Jiang, G.; Guo, X.; Fang, J.; Liu, L.; Qiao, J.; Yin, J. Polybenzimidazoles with Pendant Quaternary Ammonium Groups as Potential Anion Exchange Membranes for Fuel Cells. *J. Membr. Sci.* **2012**, *390*, 152-159.

(44) Zhang, S.; Zhu, X.; Jin, C.; Zhang, Z. Cyclodextrin Edge Functionalized Graphene Oxide Modified Poly(Phthalazinone Ether Ketone) Composite Membrane with Enhanced Properties for Anion Exchange Membrane. *Solid State Ionics* **2018**, *320*, 360-368.

(45) Tang, C. Y.; Kwon, Y. N.; Leckie, J. O. Effect of Membrane Chemistry and Coating Layer on Physiochemical Properties of Thin Film Composite Polyamide RO and NF Membranes. II. Membrane Physiochemical Properties and Their Dependence on Polyamide and Coating Layers. *Desalination* **2009**, *242* (1-3), 149-167.

(46) Kentish, S. E.; Kloester, E.; Stevens, G. W.; Scholes, C. A.; Dumée, L. F. Electrodialysis in Aqueous-Organic Mixtures. *Sep. Purif. Rev*. **2015**, *44*, 269-282.

(47) Zhang, X.; Zuo, K.; Zhang, X.; Zhang, C.; Liang, P. Selective Ion Separation by Capacitive Deionization (CDI) Based Technologies: A State-of-the-Art Review. *Environ. Sci.: Water Res. Technol*. **2020,** *6*, 243-257.

(48) Strathmann, H.; Grabowski, A.; Eigenberger, G. Ion-Exchange Membranes in the Chemical Process Industry. *Ind. Eng. Chem. Res*. **2013,** *52* (31), 10364-10379.

(49) Palakkal, V. M.; Rubio, J. E.; Lin, Y. J.; Arges, C. G. Low-Resistant Ion-Exchange Membranes for Energy Efficient Membrane Capacitive Deionization. *ACS Sustain. Chem. Eng.* **2018**, *6* (11), 13778-13786.

(50) Jain, A.; Weathers, C.; Kim, J.; Meyer, M. D.; Walker, W. S.; Li, Q.; Verduzco, R. Self Assembled, Sulfonated Pentablock Copolymer Cation Exchange Coatings for Membrane Capacitive Deionization. *Mol. Syst. Des. Eng.* **2019**, *4* (2), 348-356.

(51) Bian, Y.; Yang, X.; Liang, P.; Jiang, Y.; Zhang, C.; Huang, X. Enhanced Desalination Performance of Membrane Capacitive Deionization Cells by Packing the Flow Chamber with Granular Activated Carbon. *Water Res.* **2015**, *85*, 371-376.

(52) Hassanvand, A.; Wei, K.; Talebi, S.; Chen, G.; Kentish, S. The Role of Ion Exchange Membranes in Membrane Capacitive Deionisation. *Membranes (Basel).* **2017**, *7* (3), 54.

(53) Wang, M.; Xu, X.; Li, Y.; Lu, T.; Pan, L. Enhanced Desalination Performance of Anion-Exchange Membrane Capacitive Deionization via Effectively Utilizing Cathode Oxidation. *Desalination* **2018**, *443*, 221-227.

(54) Lado, J. J.; Zornitta, R. L.; Vázquez Rodríguez, I.; Malverdi Barcelos, K.; Ruotolo, L. A. M. Sugarcane Biowaste-Derived Biochars as Capacitive Deionization Electrodes for Brackish Water Desalination and Water-Softening Applications. *ACS Sustain. Chem. Eng.* **2019**, *7* (23), 18992-19004.

(55) Bhat, A. P.; Reale, E. R.; del Cerro, M.; Smith, K. C.; Cusick, R. D. Reducing Impedance to Ionic Flux in Capacitive Deionization with Bi-Tortuous Activated Carbon Electrodes Coated with Asymmetrically Charged Polyelectrolytes. *Water Res. X* **2019**, *3*, 100027.

(56) Porada, S.; Zhao, R.; Van Der Wal, A.; Presser, V.; Biesheuvel, P. M. Review on the Science and Technology of Water Desalination by Capacitive Deionization. *Prog. Mater. Sci*. **2013,** *58*, 1388-1442.